ELSEVIER

Available online at www.sciencedirect.com

ScienceDirect

Desalination 206 (2007) 107–126

DESALINATION

www.elsevier.com/locate/desal

A theoretical approach on membrane characterization: the deduction of fine structural details of asymmetric nanofiltration membranes

A.R. Hassan[a], Nora'aini Ali[a]*, Norhidayah Abdull[a], A.F. Ismail[b]

[a]*Department of Science Engineering, Faculty of Sicence and Technology, University College of Science and Technology (KUSTEM), 21030 Mengabang Telipot, Kuala Terengganu, Terengganu Darul Iman, Malaysia*
Tel. +60 (9) 668-3254; Fax +60 (9) 669-4660; email: noraaini@kustem.edu.my
[b]*Membrane Research Unit, Faculty of Chemical Engineering and Natural Resources Engineering, Universiti Teknologi Malaysia, 81310 UTM Skudai, Johor Darul Ta'zim, Malaysia*

Received 1 February 2006; accepted 6 June 2006

Abstract

In this study, the effects of polymer concentration on the performances and fine structural details of asymmetric nanofiltration (NF) membranes were investigated. Based on the well known models/equations on pore flow, solution diffusion and extended Nernst–Planck, the experimental data (electrolyte/ions rejection) has been modeled. Spielger–Kedem equations were used to determine the membranes parameters such as reflection coefficient, solute permeability and steric hindrance effects. Employing steric hindrance pore model (SHP) model and Teorell–Meyer Sievers (TMS) model, important membranes structural details in terms of effective pore radius, effective charge density and ratio of effective membrane thickness to membrane porosity have been measured. From the modeling results, it was found that the polymer concentration can influence the membrane performances by varying of structural details. Through the observation using scanning electron microscopy (SEM), it was shown that the produced membranes exhibited a finger-like structure. According to the results obtained from the modeling, these membranes are in range of the commercially available NF membranes.

Keywords: Nanofiltration; Theoretical model; Polysulfone; Structural details; SEM

*Corresponding author.

Presented at EuroMed 2006 conference on Desalination Strategies in South Mediterranean Countries: Cooperation between Mediterranean Countries of Europe and the Southern Rim of the Mediterranean. Sponsored by the European Desalination Society and the University of Montpellier II, Montpellier, France, 21–25 May 2006.

0011-9164/07/$– See front matter
doi:10.1016/j.desal.2006.06.008

1. Introduction

Nanofiltration (NF) membrane is a relatively new class of membranes which consist in a thin separation layer with pore sizes in the range of 1–10 nm, and their significant performances are particularly between UF and RO membranes. Another extraordinary feature of NF membranes is they are charged either positively or negatively depending on their materials [1,2]. Bandini et. al suggested that the charge of membrane is partially stimulated by electrolyte solutions kept in contact with the membrane itself [4]. Considering these features, membrane structures can be assumed as a bundle of charged capillaries with a pore radius on the nanoscale [3]. Therefore, NF membrane separation has been applied in the broadly applications such as the removal of salts in water treatment, drinking water treatment, environmental protection and the fractionation of salts and small molecules. However, the transport mechanism through these membranes is not yet clarified in a sufficient way and is still being debated.

Many authors have reported that the possible mechanisms for the NF membranes essentially depend on a combination several principles including size exclusion, charge exclusion, sometimes referred to as dielectric exclusion [5]. The uncharged solutes are rejected relatively by a sieving effect and fractional forces. Sieving (steric hindrance) effect is a function of the size exclusion where solutes with a larger molecular weight cut-off (MWCO) in the range of 200–10,000 Da will be retained Additionally, the transport mechanism of uncharged solute is contributed via convection due to a pressure difference and by diffusion due to transported solutes from one part of a system to another through a concentration gradient across the membrane [6]. This mechanism is relatively simple, easy and well-understood.

At the same time, in the case of charged solutes, the mechanism is mainly controlled by the charged exclusion (Donnan effect) which involves the interaction between the rejection of co-ions and the fixed electric charges attached to membrane matrix. The Donnan effect is marked by a characteristic dependence of rejection on the electrolyte valence type — an increase with the increasing charge of co-ions (which have the same charge of the membrane) charge and decrease with the increasing of charge of counter-ions [7]. The counter-ions will be attracted when the charge membrane is in contact with the electrolyte solution. Meanwhile, the co-ions are repulsed by the membrane surface and provide the electroneutrality condition.

Schaep et al. interpreted the Donnan effect as referred to a potential difference at the interphase (the phase between the membrane and the solution). This phenomenon is present when a charged membrane is in contact with the electrolyte solution. The membrane phase constitutes higher concentration of counter-ions than co-ions. The Donnan effect leads to preventing the movement of counter-ions to the solution and co-ions to the membrane phase. According to electroneutrality of the membrane, rejection of counter-ions is required which represented as salt rejection [8].

Currently, the transportation performance of NF membranes is the same as that UF and RO membranes that can be described with phenomenological equations by non-equilibrium thermodynamic model [9]. This model assumes that the membrane is a black box. This approach can be applied when the structure of the membrane is not known and no information about the transport mechanism can be obtained. Therefore, the critical main point in this issue is to develop a theory to evaluate the structural parameters and the electrical properties of NF membranes and examine the transport mechanism performances of NF membranes by applying the transport models.

Nowadays, there are some well-known theoretical models of mass transfer through NF membranes. These models are based on diffusion, adsorption, ion exchange, ion coupling, concentra-

tion polarization or other mechanisms of mass transfer. Each model has been established for specific conditions. However, none of the existing model is valid for wide range applications. The key points of these models are based on either the structural parameters or the electrical properties of membrane. Some assumptions have been made according to the steric hindrance pore (SHP) model and Teorell–Meyer–Sievers (TMS) model where the membrane is considered a charged porous layer, partitioning effects are described by steric hindrance and electrostatics, and mass transfer through the membrane is based on the extended Nernst–Planck equation. These assumptions will be utilized to estimate the properties of a membrane.

Nakao and Kimura eliminated the wall correction factors from the modified pore model and successfully proposed the SHP model. The membrane parameters (reflection coefficient σ and solute permeability, *P*) were estimated by relating to the structural parameters which recognized both the steric-hindrance effect of solute and the interaction between solute and pore wall [10].

This model was employed to predict prominent structural parameters of a UF membrane in terms of pore radius, r_p and the ratio of membrane porosity to membrane thickness, $A_k/\Delta x$.. The structural parameters were obtained by a permeation experiment carried out in aqueous solutions of single organic solutes. The pore radii of charged UF membranes were estimated from the SHP model to be a few nanometers, which seems to be larger than those of NF membranes [8]. Based on the SHP model, Wang and co-workers [9] have personalized the SHP model to investigate the structural parameter of thin film composite NF membrane by using the aqueous solution of neutral solutes in permeation experiment. From the permeation experiment with sodium chloride, they interpreted the effective charged density X_d that can be correlated with q_w, using r_p, as a function of salt concentration. They concluded that the permeation of a single neutral solute across the NF membrane only took place by steric hindrance effects. Indeed, when the membrane pore radius is much larger compared to the electrolyte ion size, only electrostatic effect took place for the permeation of electrolytes. Besides, Deen et al. introduced the steric-hindrance factors into molecular ions across the glomerular capillary wall fixed negatives charges. The effects of Donnan electrical potential and the steric-hindrance factors on the concentration distribution were defined [9].

To estimate the data of the transport of single solute and solvent through the NF and RO membranes, the Spiegler–Kedem model can be applied [11]. This model accounts for the variability of the concentration profile at large fluxes and high concentration gradients. In 1989, Perry and Linder attempted to calculate the effect of Donnan in a charged NF membrane by the extended Spiegler–Kedem model [12]. In addition, they also analyzed an RO membrane and successfully postulated a negative rejection of sodium chloride in the separation of water-soluble organics ions of a molecular weight lower than a few hundred Dalton from sodium chloride solutions [9].

Schirg and Widmer investigated the effect of feed concentration on salt permeability by the extended Spiegler–Kedem model with correlation to a power law [13]. They proposed a method to account the selectivity of the dye and salt for an NF membrane of aqueous dye–salt mixed solutions. In this method, the optimum selectivity at a certain flux was measured [9]. Therefore, they provided a new assumption where the larger charged solutes are retentated completely in the simplified system. According to the Spiegler–Kedem model which was combined with the film theory, Chatterjee and co-workers postulated the mass transfer coefficient through the RO membrane for application to brackish water and seawater filtration, respectively [13]. Wadley et al. also used the Spiegler–Kedem model which was combined with the film theory to estimate the performance of a binary solute system such as sodium chloride and organics. They mentioned

both of solutes as semi-permeable across the membrane. Meanwhile, total osmotic pressure gradient exerted by the concentration gradient of each solute totally influenced the volume flux across the membrane [15]. Ahmad and co-workers suggested that the Spiegler–Kedem model can be extensively applied in single solute systems and binary solutes systems. They assumed the one solute of that system impermeable to the membrane and the solute–solute interactions were ignored [16].

Schaep et al. explained that the electrostatic interaction took place when the membrane charges where in contact with the charged components. For this reason, the SHP model was particularly used for the permeation of a single neutral solute and it was not suitable for application of salt retention [17]. Teorell–Meyer–Sievers (TMS) model can be interpreted using the electrical properties of the membrane. This rigorous model assumes a uniform radial distribution of fixed charges and mobile species. Bowen et al. explained that these assumptions are suitable when applied at low concentration and pores smaller than 2 nm [18]. This model is generally used to explain the transport mechanism in NF membranes in terms of the electrostatic effects for the permeation of electrolyte (sodium chloride). The eventual dependences of the transport coefficient on the virtual concentration that are accounted automatically, is the obvious advantage of TMS model. In a previous study, the TMS model was used in order to estimate electrolyte solution across charged UF membranes. The experiment was carried out in aqueous solutions of both single electrolyte and mixtures by combining the extended Nernst–Planck equation.

In the literature, Osterle et al. attempt to validate their mechanistic model by developing the space-charge model in terms of electrokinetic phenomena in charged capillaries [19]. The space-charge model suggests that there is a radial distribution of the potential and concentration gradient across the pores (two dimensional approaches). The main hypothesis of this model is that an NF membrane consists of a straight capillary having charge on its surface. They treated ions as point charges. So the steric effects of the size of ions were neglected. The basic equation of this model included the Nernst–Planck equation for ion transport, the non-linear Poisson–Boltzmann equation for ion concentration and radial distribution of electric potential, and the Navier–Stokes equation for the force balance in narrow pores relative to pore length.

Wang and co-workers investigated and compared between the space-charge models and Spiegler–Kedem in order to predict the rejection of single electrolyte solutions at an NF membrane [3]. These models provided a more stable numerical solution. However, the major disadvantage of these models is that the numerical solution of this models required solving by computationally expensive, even though with simplifying assumptions. In addition, these models derived the steric effects and friction interactions. Therefore, the contribution is obviously important for the NF membrane, especially commercial membrane. Thus, these interactions can be calculated for in other manner [20].

Some authors studied other models such the Donnan steric pore model (DSPM). This model was developed by Bowen and co-workers and successfully characterized the membrane properties and membrane structure [18]. The DSPM model uses the extended Nernst–Planck equation to elaborate ion transport and the steric Donnan equilibrium model to explain ion partitioning across the membrane. However, the disadvantage of this model is could not be applied by fixing a certain value as a constant to find another one. These might affect the accuracy of the other parameters. Consequently, it is possible that the whole modeling results will also be affected [1,2].

In this study, it is proposed to use three polysulfone NF membranes with different polymer concentrations to study the effect of steric and charge on the separation performance and fine

structural details of NF membranes. By using the same polymeric materials, an uncertainty imposed by the membrane material upon separation performances can be eliminated. Polymer concentration illustrated a great effect on morphology and liquid–liquid separation performances of membranes. The polymer concentration most influenced the diffusion of solvent–non-solvent in the precipitation rate. Membranes with high polymer concentration (high viscosity) have a tendency to make the precipitation rate slower. As a result, membranes with dense and thick skin layer supported by a cell sublayer produced [21,22].

The membrane performances were employed by the permeation experiments of aqueous NaCl solution to estimate the membrane properties and membrane structures. Considering the SHP model and Spiegler–Kedem model, the transport performance of NF membrane such as r_p and $\Delta x/A_K$ can be predicted. Whereas, the Teorell–Meyer–Sievers model were applied to investigate the electrostatic effects such as X_d, and the ratio of effective charge density to concentration of bulk solution ξ.

2. Theoretical approach

The theoretical approach for the UF, NF and RO membranes is based on the irreversible thermodynamic (IT) model [1–3,9]. Therefore, the filtration process involving the free energy is dissipated and entropy is continuously produced. Consequently, the model can be used to interpret the membrane transport mechanism based on solute–solvent, solute–membrane and solvent–membrane. Initially, the description of the membrane performance can be measured through the dissipation function, even though this approach may not address the mechanism of rejection. Kedem and Katchalsky (KK) originally derived this type of model to describe the flow of solution and solute through the membrane as follows [23].

$$J_v = L_p\left(\Delta P - \sigma\Delta\pi\right) \tag{1}$$

$$J_s = P_s\left(c_m - c_p\right) + \left(1-\sigma\right)J_v c \tag{2}$$

Then, the KK model was modified by Speigler–Kedem (SK) [24]. They used a differential form to reformulate a similar set of equations in order to overcome the limitation found in this model. In this model the membrane is treated as a black box as the membrane structure is not known and there is no information about its transport mechanism. The key points of the SK model are considered as the variability of the concentration profile at large fluxes and high concentration gradients. The correction of this model is calculated based on the average concentration inside the membrane which is shown in Eq. (3). Therefore, the SK model indicates that transport through membrane is characterized by three parameters which are solvent (water) permeability, solute permeability and reflection coefficient.

$$J_s = -P'\left(\frac{dc}{dx}\right) + \left(1-\sigma\right)J_v c \tag{3}$$

According to Eq. (3), P' is local solute permeability expressed as $P' = P \times \Delta x$. Integrating Eq. (3) across the membrane thickness yields Eq. (4).

$$R = 1 - \frac{c_p}{c_m} = \frac{\sigma\left(1-F\right)}{\left(1-\sigma F\right)} \tag{4}$$

$$F = \exp\left(-\frac{1-\sigma}{P}J_v\right) \tag{5}$$

Eq. (4) is a well-known Spiegler–Kedem equation. σ and P_s can be determined solely by experimental data, R, as a function of J_V by a best-fit method. For this reason, several transport mechanisms have been suggested to predict structural parameters and the electrical properties of a membrane [1].

According to Eq. (7), Schaep et al. mentioned that the retention increased with the increasing of

water flux, and a limiting value of σ was obtained at an infinitely high water flux [8]. Generally, the convective solute transport is totally hindered or no transport by convection takes place at all conditions when σ is equal to 100%. This condition is appropriate to apply on membranes which have a dense structure and no pores are available for convective transport. These membranes have been recognized as reverse osmosis membranes. RO membranes may have retention lower than 100%. It has been shown that the transportation performance of these membranes is described by the solution diffusion [16]. In this study, NF membranes which have pore structure were analyzed. Therefore, it is important to estimate the reflection coefficient σ below 100% when the solutes are small enough to enter the membrane pores.

2.1. Steric hindrance pore (SHP) model

An ionic flux can be described by a common assumption of the extended Nernst–Planck equation. Indeed, some authors have found the steric hindrace effects by rearranging the extended Nersnt–Planck equation in order to estimate the ion flux inside a charged NF membrane as expressed in Eq. (6).

$$J_i = v_i k_i \left[H_{F,i} u_x c - H_{D,i} D_i \left(\frac{dc}{dx} + c \frac{z_i F d\phi}{RT dx} \right) \right] \quad (6)$$

The H_F and H_D parameters are for steric hindrance and frictional forces that impede convective and diffusive transport, respectively, and are expressed by the SHP model as in Eqs. (7)–(12).

$$\sigma = 1 - H_F S_F \quad (7)$$

$$P_s = H_D S_D D_S \left(A_K / \Delta x \right) \quad (8)$$

$$H_D = 1 \quad (9)$$

$$H_F = 1 + \frac{16}{9}\eta^2 \quad (10)$$

$$S_F = (1-\eta)^2 \left[2 - (1-\eta)^2 \right] \quad (11)$$

$$S_D = (1-\eta)^2 \quad (12)$$

2.2. Teorell–Meyer–Sievers model

The Teorell–Meyer–Sievers (TMS) model is a rigorous approach to describe the membrane electrical properties in terms of the effective charge density, X_d and electrostatic effects, ξ. This model has been extensively used to explain the transport mechanism in NF membranes considering the electrostatic effects for the permeation of electrolyte (sodium chloride). The TMS model assumes a uniform radial distribution of fixed charges and mobile species. Bowen et al. explained that these assumptions are suitable at low concentrations and in pores smaller than 2 nm. The modeling results clearly show that the electrolyte ions have a larger size than the membrane pore radius. The TMS equation can be rewritten as in Eqs. (13) and (14) [17].

$$\sigma_{\text{salt}} = 1 - \frac{2}{(2\alpha - 1)\xi + (\xi^2 + 4)^{1/2}} \quad (13)$$

$$P_{\text{salt}} = D_S (1 - \sigma_{\text{salt}}) \left(\frac{A_K}{\Delta x} \right) \quad (14)$$

where $\xi = X_d/c$, ξ is an electrostatic effect and X_d is called the fixed charged density.

3. Experimental

3.1. Materials

In this study, the membranes were fabricated from ternary casting solution consisting of polysulfone (PSf) as a polymer, N-methyl-2-pyrrolidone (NMP) as a solvent and polyvinylpyrrolidone (PVP K30) as a non-solvent additive. Tap water was used as a first coagulation medium and methanol as a second coagulation medium. Pure

water and sodium chloride (Aldrich) were used in permeation experiments.

3.2. Membrane fabrication

Asymmetric PSf flat sheet membranes were prepared by the phase inversion technique. Homogenous solutions of the membrane casting polymers in NMP and PVP were prepared. They were subjected to different levels of polymer concentrations by stirring for a few hours. Membrane dope formulations used in this study are shown in Table 1.

Casting processes were performed by a casting machine. The homogenous solution was poured onto a glass plate and spread with a casting knife at an approximately constant shear rate 87.5 s^{-1}. The nascent membranes were evaporated at room temperature for 10 s. Then, all membranes were immersed in water coagulation bath overnight. After the immersion step, the membranes were transferred into methanol (8 h) for solvent-exchanged process to ensure that the excess solvent and water-soluble polymer were totally removed. Finally, the membrane was dried at room temperature.

3.3. Permeation experiment

The permeation experiment was performed using dead-end cell filtration supplied by Sterlitech HP4750 stirred cell with 300 mL processing volume and effective permeation membrane area of 14.6 cm^2. This experiment was done by using a standard feed solution; pure water (to obtain pure water permeability and to ensure that the membrane used was stable) and sodium chloride 0.01 M (0.1711 mol/m^3) to determine the membrane performances in terms of rejection rate and fluxes. The experiments were conducted at ambient temperature (27°C). The operating pressures were between 0–16 bar, in order to obtain 0–10.0 $\times 10^{-6}$ $m^3/m^2.s$ flux range, as suggested in the literature [18]. The solution was stirred magnetically using a magnetic stirrer (Model H1303N) to avoid concentration polarization phenomena above the membrane surface during the filtration process. In this study, concentration polarization was evaluated taking into account real rejection. In all experiments, samples of both permeate and retentate were taken and conductivity was checked by a conductivity meter (CyberScan CON 510 Conductivity/TDS Bench Meter model).

Table 1
Membrane dope formulations with different polymer concentrations

Membrane	Composition (PSf/NMP/PVP) (%)
PSF18	18/75/7
PSF20	20/73/7
PSF23	23/70/7

3.4. Membrane characterization

Generally, all adopted models of the NF membrane transport are essentially based on the pore flow model and solution–diffusion model. These approaches have been applied to explain the permeation mechanism. The pore flow model assumes that the permeant transport occurs by a pressure-driven convective flow through tiny pores. Separation can be obtained when one of the permeants is excluded from some of the pores in the membrane through which other permeants move. The solution–diffusion model can be explained according to differences in permeability that consists both of solubility and diffusive components. Separation occurs when the permeants dissolve in the membrane matrix and then diffuse across the membrane down a concentration gradient.

3.4.1. Determination of the pore radius on the membrane surface

A statistical analysis of all experimental data is presented in Table 2. The data were obtained from the permeation experiments of three NF membranes with varying the polymer concen-

Table 2
The modeling results

Membranes	Pressure (bar)	P_s [$\times 10^{-7}$]	Δx [$\times 10^{-3}$]	A_K	r_P	$\Delta x/A_K$ [$\times 10^{-3}$]	X_d (–ve)	ξ (–ve)
PSf 18	4	0.90	17.82	1.59	2.52	11.23	13.89	1.93
	8	1.24	12.95	1.82	2.01	7.13	13.71	1.89
	12	1.80	8.93	2.09	1.69	4.28	13.64	1.69
	16	2.96	5.44	2.52	1.40	2.15	13.40	0.89
	Average	1.73	11.28	2.00	1.91	6.20	13.66	1.60
PSf 20	4	0.60	26.71	2.00	1.77	13.34	17.05	2.05
	8	1.01	15.88	2.23	1.57	7.12	16.97	1.99
	12	1.52	10.59	2.47	1.43	4.28	16.87	1.83
	16	1.65	9.77	2.93	1.25	3.33	14.83	1.81
	Average	1.20	15.74	2.41	1.51	7.02	16.43	1.92
PSf 23	4	0.22	71.83	2.79	1.30	25.79	21.11	2.44
	8	0.25	63.38	2.95	1.24	21.48	21.03	2.41
	12	0.37	43.95	3.00	1.23	14.65	20.75	2.38
	16	0.45	35.44	3.28	1.16	10.79	18.07	2.25
	Average	0.32	53.65	3.01	1.23	18.18	20.24	2.37

trations. Prior to the permeation experiment (fluxes and rejection rate) the membranes were subjected to an aqueous solution of sodium chloride with concentration of 0.01 M (0.1711 mol/m^3). Firstly, the dependency of the Stokes–Einstein equation ($r_s = kT/6\pi\mu D_s$), the Stokes radii of the solute can be determined. The literature of ionic in diluted aqueous solution is shown in Table 3.

Secondly, the coefficient of η was estimated. As in Eqs. (10)–(12), η is defined as the ratio of solute radius (r_s) to pore radius (r_p). When the ratio of pore radius to pore size is increased, it could reflect the increasing of the steric hindrance effect and also the increasing of reflection coefficient to a value of 100% if r_s/r_p is equal to 1. In this study, the values of the reflection coefficient are converted into percentage values as shown in Table 4. However, if the rejection data and the solute radius are known, the pore radius can be predicted. This is important because the NF pore radius is very difficult to measure if those membranes are indeed porous. Therefore, according to the SHP model, the membrane pore radius can be calculated. This model suggests that the pore radius is uniform and in reality a pore radius distribution will exist. A simple estimation of the pore size can be obtained by considering the uniform pore size distribution of the membrane, and it is expressed as a simple analytical function of η in Eq. (15) [25].

Table 3
Ions, ion atomic or molecular weights, ion diffusivities and Stokes radii

Ionic type	AW/MW	D_s [$\times 10^{-9}$](m^2/s)	r_s
Na^+	23.99	1.33	0.184
Cl^-	35.45	2.03	0.121
NaCl	59.44	1.33	0.520

$$\sigma = 1 - \frac{c_p}{c_r} = 1 - \frac{2(1-R)}{2-R} = f(\eta) \tag{15}$$

The increase of σ values and the rejection rate

Table 4
Numerical results, membrane parameters obtained from SHP model and the convection and diffusion steric parameter at different polymer concentrations

Membranes	Pressure (bar)	η		H_F	S_F	S_D
PSf 18	4	0.21	0.07	1.08	0.86	0.63
	8	0.26	0.11	1.12	0.80	0.55
	12	0.31	0.15	1.17	0.73	0.48
	16	0.37	0.21	1.24	0.64	0.40
	Average	0.29	0.13	1.15	0.76	0.51
PSf 20	4	0.29	0.14	1.15	0.75	0.50
	8	0.33	0.17	1.19	0.70	0.45
	12	0.36	0.20	1.24	0.65	0.40
	16	0.42	0.26	1.31	0.57	0.34
	Average	0.35	0.19	1.22	0.66	0.42
PSf 23	4	0.40	0.24	1.29	0.59	0.36
	8	0.42	0.26	1.31	0.56	0.34
	12	0.42	0.27	1.32	0.56	0.33
	16	0.45	0.30	1.36	0.52	0.30
	Average	0.42	0.27	1.32	0.56	0.33

is mainly affected by the increase of the polymer concentration. It can be noted that this finding is greatly used as an indicator of the membrane performance and pore size distribution.

Then, the membrane parameters such as η, H_F, S_D and S_F were calculated. The values of the reflection coefficient were predicted by employing the Spiegler–Kedem model. Eqs. (4) and (5) actually represent a basis of solution–diffusion models [26]. Based on the SHP model, these parameters take place in the NF membrane transport mechanism which performs as the diffusion and convection factors. Table 4 shows the values of membrane parameters and steric-hindrance factors which preferentially contributed to the electrolytes transport across NF membranes in terms of diffusion and convection conditions.

3.4.2. Determination of the solute permeability and membrane thickness

According to the SHP model, the reflection coefficient considering the steric and hindrance factors (H_F, H_D, S_F and S_D) could be estimated. The factors are referred to a convection and diffusion steric parameter to the membrane properties and membrane performance. Subsequently, the solute permeability and membrane thickness can be evaluated based on Eq. (8). The membrane thickness can be deducted based on the equation $P_s = D_s/\Delta x$ where P_s is a solute permeability, D_s is a diffusion coefficient (1.61×10^{-9} m^2/s) and Δx is a membrane thickness. The results of solute permeability and membrane thickness are tabulated in Table 5.

3.4.3. Determination of membrane porosity and the ratio of effective membrane thickness to membrane porosity

The solute permeability, effective membrane thickness and solute diffusion coefficient are parameters that are required for determining the membrane porosity. Based on Eqs. (7)–(11) as well as a summary of the effects of parameters in Table 5, the membrane porosity can be predicted. In order to determine the ratio of the effective membrane thickness to membrane porosity, the SHP model

Table 5
Flux and percentage of rejection of electrolytes (0.01 M NaCl)

	Pressure (bar)	Polymer concentration		
		PSf 18	PSf 20	PSf 23
Flux, J_v ($m^3.m^2/s$) [$\times 10^{-7}$]	0	0.00	0.00	0.00
	4	11.17	8.007	3.40
	8	15.99	14.007	3.95
	12	24.30	21.890	5.74
	16	43.00	25.548	7.44
	Average	23.62	17.36	5.13
Percentage of rejection, R (%)	0	0.00	0.00	0.00
	4	34.16	45.37	57.23
	8	41.04	49.70	58.94
	12	47.06	53.40	59.43
	16	54.06	58.75	61.90
	Average	44.08	51.80	59.38

was rearranged to get another equation as follows:

$$\Delta x / A_k = H_D S_D D_S / P_S \quad (16)$$

The membrane porosity and the ratio of the effective membrane thickness to the membrane porosity of three different polymer concentrations were obtained by inserting all numerical values into Eq. (16).

3.4.4. Determination of the effective membrane charge density and the ratio of the fixed charge density to the bulk concentration

Eqs. (14) and (15) are well documented as the TMS model which is adapted to predict the effective membrane charge density, X_d. It should be noted that the SHP model only enables consideration of the steric hindrance effects. According to the permeation experiment data, the membrane charge density is an electrical property of the membrane. The TMS model considers only the electrostatic effect for the permeation of electrolytes, such as sodium chloride. In the present study, the fabricated NF membranes were considered as model charged porous membranes. Therefore, there is evidence that the electrostatic membrane–ion interactions play an important role in the ion transport of NF membranes. The electrostatic effects are represented by ξ, that is a ratio of the fixed charge density (X_d) to the bulk concentration of electrolyte (C_{total}). The theoretical results including the electrical properties are reported in Table 2. Finally, Fig. 1 shows the flowchart of the modeling procedures in order to estimate fine structural details of the membrane by using the theoretical approach.

3.5. Scanning electron microscopy (SEM)

Membrane morphology analysis was conducted using scanning electron microscope (Model JSM P/N HP4750). For this purpose, the sample of the membrane was fractured cryogenically in liquid nitrogen. The membrane specimen was then subsequently coated with gold using automatic coater (JFC 1600). After sputtering the parts with gold, they were transferred into the microscope and the cross-section can be observed under magnifications of 500×.

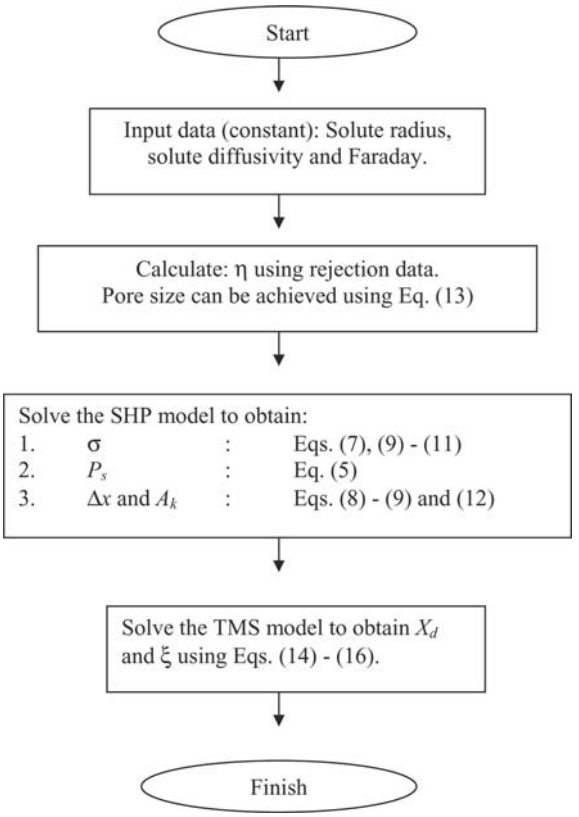

Fig. 1. Pure water flux vs. applied pressure.

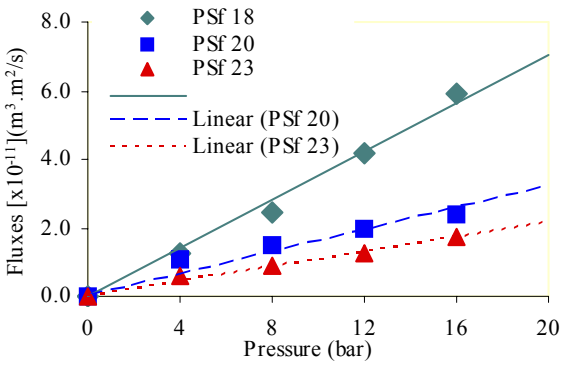

Fig. 2. Pure water permeation vs. pressure.

Table 6
Pure water fluxes

Pressure (bar)	Fluxes [10^{-6}](m^3.m^2/s)		
	PSf 18	PSf 20	PSf 23
0	0.00	0.00	0.00
4	1.23	1.08	0.60
8	2.45	1.49	0.92
12	4.17	1.97	1.24
16	5.90	2.37	1.72

4. Result and discussion

4.1. Pure water permeability

The measurements of water flux as a function of applied pressures were used to investigate the stability and hydraulic properties of NF membranes. The pure water permeability for each membrane samples was determined and is shown in Fig. 2. Table 6 shows the results of pure water permeability. The slope of the fitted line gave the values of pure water permeability of three tested membranes PSf 18, PSf 20 and PSf 23 and they were about 3.606, 1.496 and 1.213 [10^{-6}], respectively. Noticeably, the permeability of membranes decreased in the following sequence: PSf 18 > PSf 20 > PSf 23. This indicated that higher polymer concentration would lead to lesser the membrane permeability.

In all cases, pure water flux was a linear function of the applied pressure that shows a very good approximation. This result is in agreement with the Hagen–Poiseuille equation as below:

$$J_v = \frac{\varepsilon r}{8\eta}\frac{\Delta P}{\tau \Delta x} \tag{17}$$

According to the equation, the increase in water flux is proportional to the increase in the applied pressure.

Based on the pure water permeability results, we can postulate that PSf 23 has lower fluxes and is less permeable compared to PSf 18 and PSf 20 membranes. This indicates that higher polymer concentration in casting solutions would form a

denser and thicker skin layer, leading to more selectivity but less productivity. This finding is supported by the results of the theoretical approach and SEM micrographs where the membrane with high polymer concentration shows a less porous substructure. It will be explained further in section 4.3. All of the fabricated membranes have shown significant water flux in the range between UF and RO membrane water fluxes [17]. The great advantage of the NF membrane is a relatively high water flux at a low applied pressure which has a high potential of using less energy.

4.2. Modeling results and analysis

Membrane separation performance is discussed in terms of selectivity (percentage of ion chloride rejection) and productivity (fluxes for a range of operating pressures). Fig. 3 shows membrane separation performances using sodium chloride (NaCl) with 0.1711 mol/m^3 concentration and Table 5 shows the results of fluxes and rejection of sodium chloride. Table 5 and Table 6 show clearly that the permeate flux was slightly lower compared to the pure water flux for all conditions. As the pressure increased, the rejection also increased. According to the experimental data shown in Fig. 3, the fluxes and rejections change in the following manner: $R_{PSf23} > R_{PSf20} > R_{PSf18}$, where the flux and the percentage rejection of sodium chloride increased with the increase of polymer concentration. PSf 23 shows the highest sodium chloride rejection (R_{PSf23} = 61%) with the lowest flux. This trend shows that the membranes would have a denser and thicker skin layer with the increase of polymer concentration. Better selectivity for solute solution can be achieved due to the denser and thicker skin layer of the membrane [16]. Detailed explanation on the changes in the fine structural details can be seen in Figs. 4–9. All numerical results in terms of membrane parameters (which were obtained from the SHP model) and the convection and diffusion steric parameters at different polymer concentration are shown in Table 4.

The changes of membrane structural details that had been determined are based on the theoretical approach and illustrated in Table 2. According to the Spiegler–Kedem equation, the reflection coefficient and solute permeability were determined by the best fit method. Then, based on the SHP model, the effective pore radius, the membrane porosity, the membrane thickness and ratio of the membrane thickness to the membrane

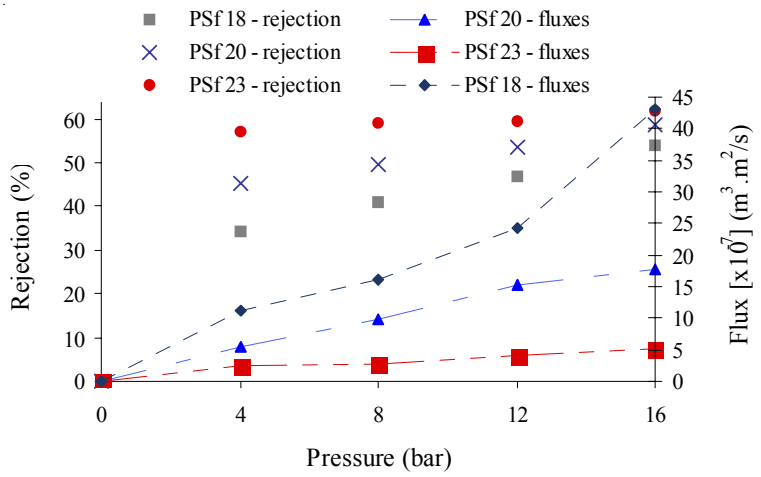

Fig. 3. Rejection and fluxes vs. applied pressure.

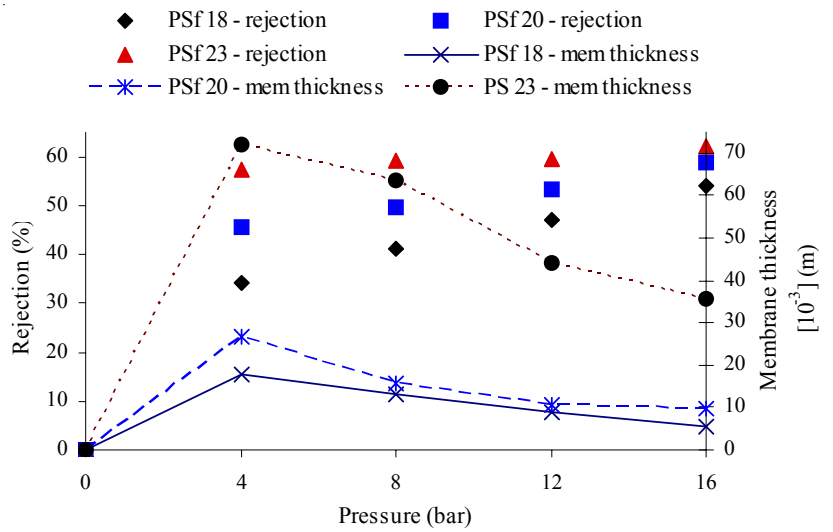

Fig. 4. Rejection and membrane thickness vs. applied pressure.

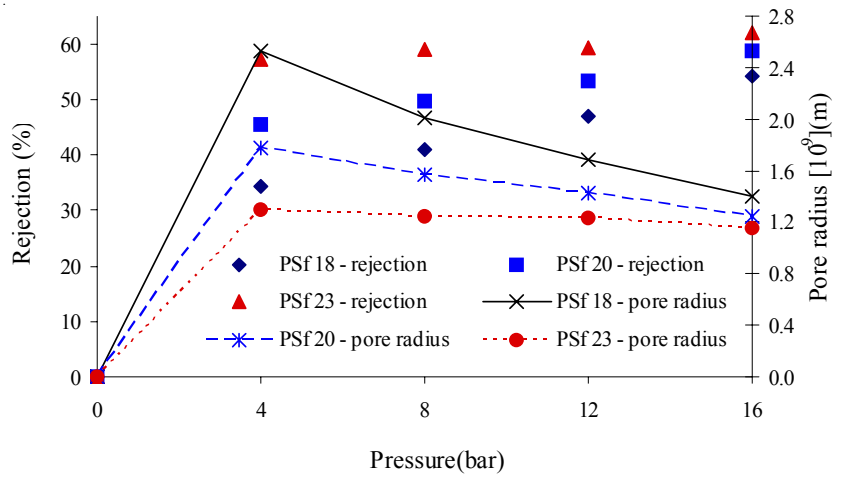

Fig. 5. Rejection and pore radius vs. applied pressure.

porosity can be predicted. By applying the Teorell–Meyer–Sievers model, the electrostatic properties of the membrane in terms of effective membrane charge density and the ratio of the effective membrane density to the bulk charge concentration could be predicted.

The results of the theoretical approach to NF membranes revealed that the higher polymer concentration indicated the higher membrane thickness but smaller pore radius of membranes as shown in Figs. 3–6. In addition, Fig. 7 is plotted in order to understand the relation between the membrane thickness and membrane porosity. As the membrane thickness increased, the membrane

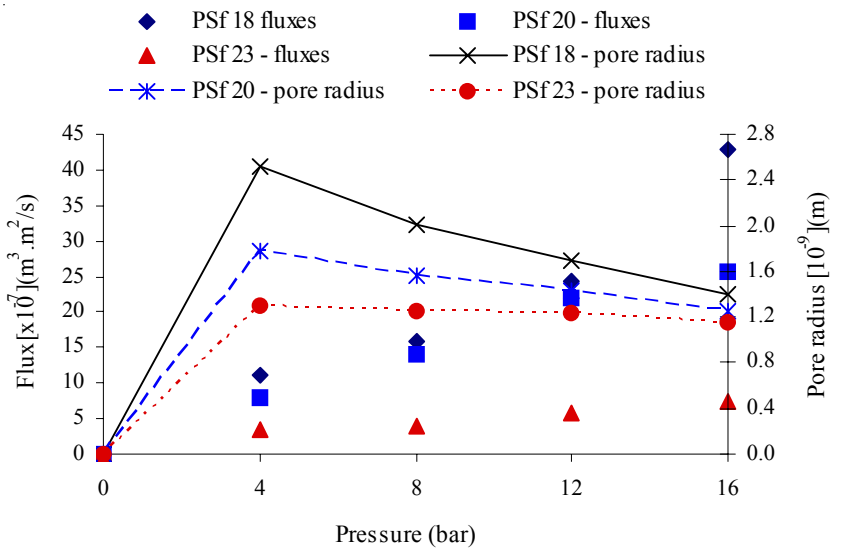

Fig. 6. Fluxes and pore radius vs. applied pressure.

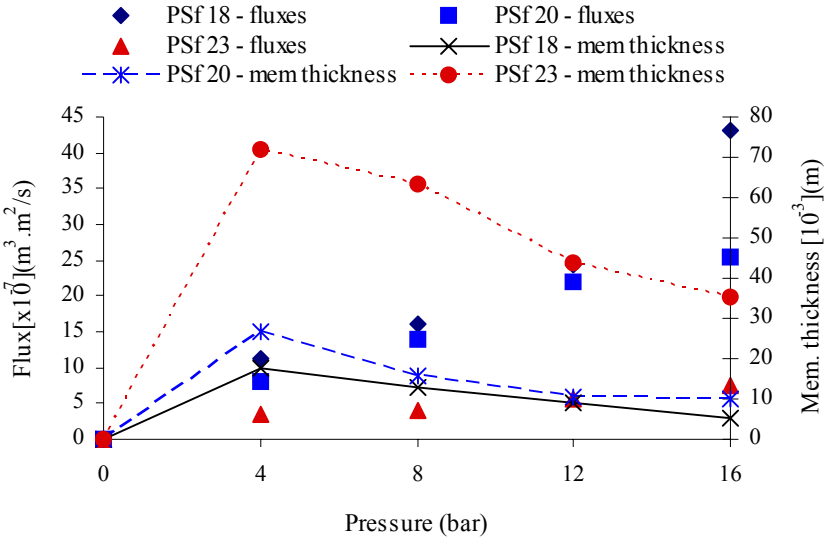

Fig. 7. Fluxes and membrane thickness vs. applied pressure.

porosity also increased, which exhibited the proportional relation. Meanwhile, Fig. 8 illustrates that the membrane pore radius shows inverse results. Therefore, it would result in a higher rejection and lower fluxes. The pore radii obtained in this study were of the magnitude of typical pore radii of the NF membrane separation range. The reason of this finding could be attributed to the fact that casting solution with the high level of polymer concentration accelerated the solution

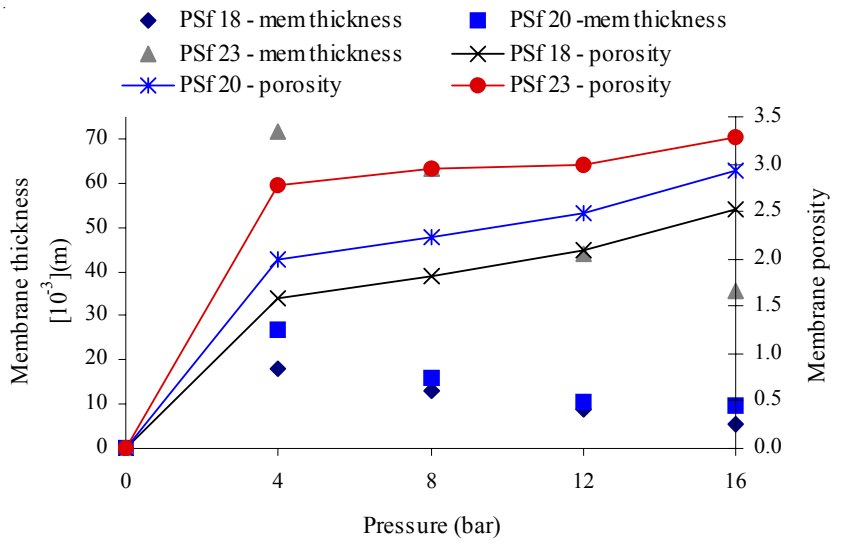

Fig. 8. Membrane thickness and membrane porosity vs. applied pressure.

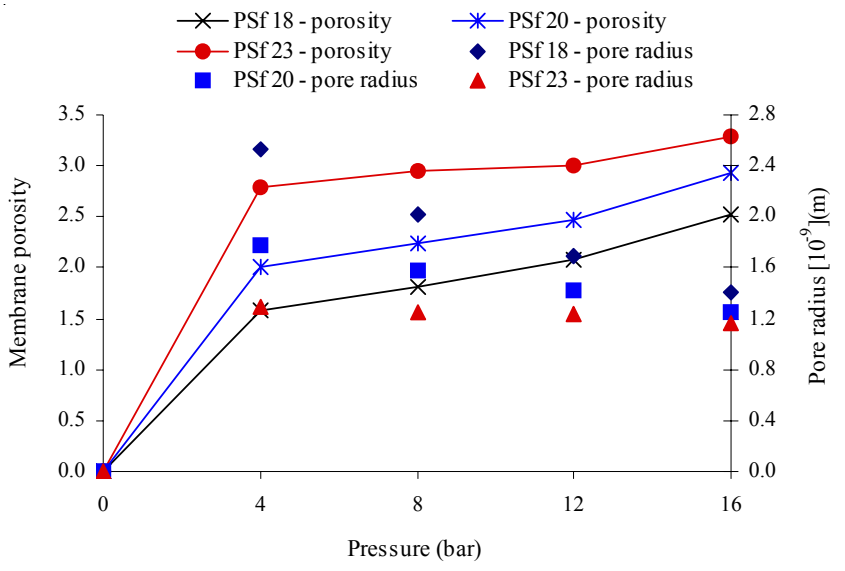

Fig. 9. Porosity and pore radius vs. applied pressure.

viscosity which retarded the diffusional exchange rate of the solvent (NMP) and non-solvent (water) in a sublayer.

Therefore, the expected precipitation rate would occur slowly. The fast phase separation is at the outer skin layer and the slow phase separation is at the sublayer. As a result, asymmetric membranes with a dense and thick skin layer supported by a closed cell sublayer could be formed as shown in SEM micrographs. In Fig. 9, the in-

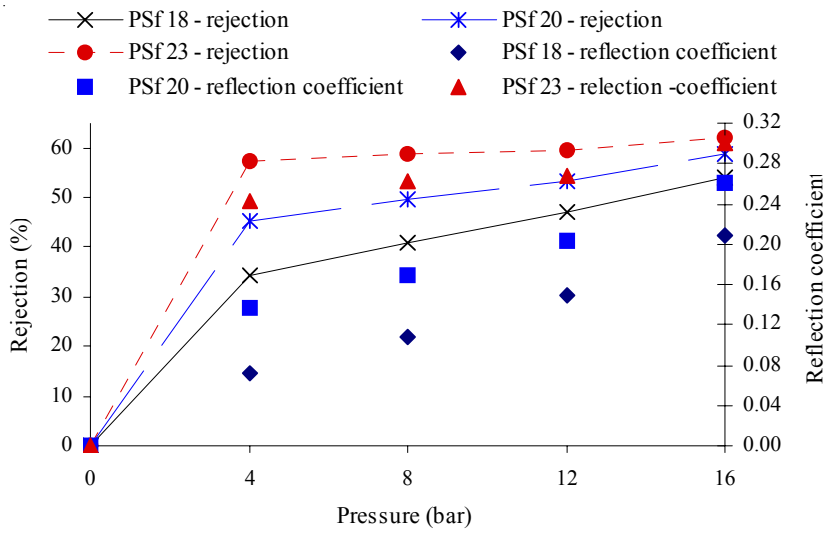

Fig. 10. Rejection and reflection coefficient vs. applied pressure.

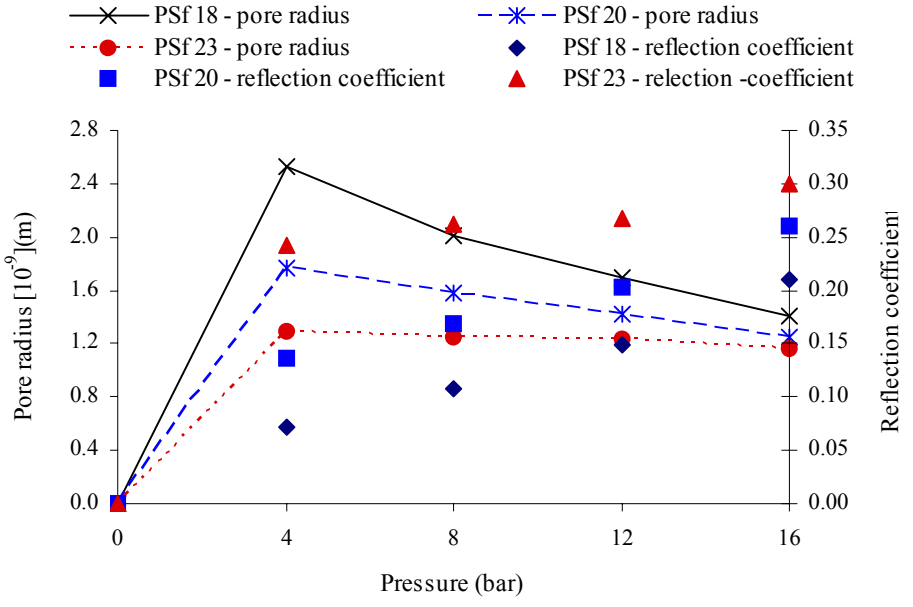

Fig. 11. Pore radius and reflection coefficient vs. applied pressure.

crease of polymer concentration followed by the increase in the rejection rate mainly caused the increase of the reflection coefficient values. Meanwhile, the polymer concentration decreased the membrane pore size as shown in Fig. 10. This finding proved that the reflection coefficient is proportional to the rejection and disproportional to the membrane pore radius.

The sodium chloride rejection is essentially due to two dominant membrane parameters such as effective pore radius and the ratio of the effective charge density to the bulk electrolyte concentration. With the emphasis on the investigation of the ratio of the effective charge density to the bulk electrolyte concentration, the TMS model was adapted to the experimental data, as listed in Table 2. The increase of the membrane charge resulted in the increase of NaCl rejection. This observation is strongly based on the relative symmetry between Na^+ and Cl^- ions in terms of charge and size ion. The rise of the positive charge magnitude on the membrane exhibited the rise of sodium chloride rejection in parallel with the increase of the negative charge magnitude.

The comparison between fabricated membranes and 29 commercial NF membranes in terms of an effective pore radius, the ratio effective charge density to bulk electrolyte concentration and the ratio of membrane porosity to membrane thickness is shown in Table 7. It clearly shows that the fabricated NF membranes have a similar potential as that of commercial NF membranes. Thus, these fabricated membranes have a great platform in a wide range of applications such as the removal of natural organic matter (NOM) in water supplies. A major fraction of NOM is contributed by humic substances (humic and fulvic acid). According to the description of humic and fulvic acids, NOM could be removed by NF membranes sufficiently due to their range of MWCO between 100–500 Da [25].

Table 7
Summary of the characteristics of 29 commercial NF membranes and fabricated membranes*

Parameters	r_p (nm)	ξ^a
Minimum	0.39	–1.5
Mean	0.66	–9.2
Maximum	1.59	–44.5
PSf 18*	1.84	–1.60
PSf 20*	1.49	–1.92
PSf 23*	1.23	–2.37

According to Figs. 3–10, the optimum applied pressure can be reached at 4 bar. Using this pressure, the membrane properties such as sodium chloride rejection, fluxes, pore radius, membrane porosity and membrane thickness, are suggested as optimum values. The critical membrane properties turn to inverse if the pressure is higher than the optimum pressure. Moreover, the polymer concentration of PSf 20 membrane was illustrated as the optimum polymer concentration. PSf 20 membrane showed the optimum salt rejection (R_{PSf20} = 45%) and flux (0.801×10^{-6} $m^3/m^2.s$) at an applied pressure of 4 bar. It is postulated that PSf 20 membrane can be considered as a superior membrane due to the trade-off between the moderate flux and quite high rejection percentage. In order to predict the best conditions for the fabrication of high-performance membranes and to estimate the fine structural details of membranes, an optimum polymer concentration and applied pressure are required to be determined first.

4.3. Membrane morphology

The cross-sectional image in Fig. 12 clearly shows that occurrence, location, size and uniformity of the pore strongly depend on the polymer concentration: 18%, 20% and 23% (w/w). The fabricated membranes show the expected typical asymmetric structure which comprises a skin layer that is very well developed and supported by a porous support layer with macro-voids. In each case, the top of the film structure (i.e. the side that was never in contact with the glass casting plate) is at the top of the micrograph. All membranes have no pores on the top surface, while membrane pores decreased in diameter from the bottom to the top surface of the membrane. This condition allowed the salt rejection occurrence at a very thin top layer and relatively high fluxes [21].

Membranes with lower polymer concentration (lower viscosity), i.e. PSf 18 and PSf 20, having

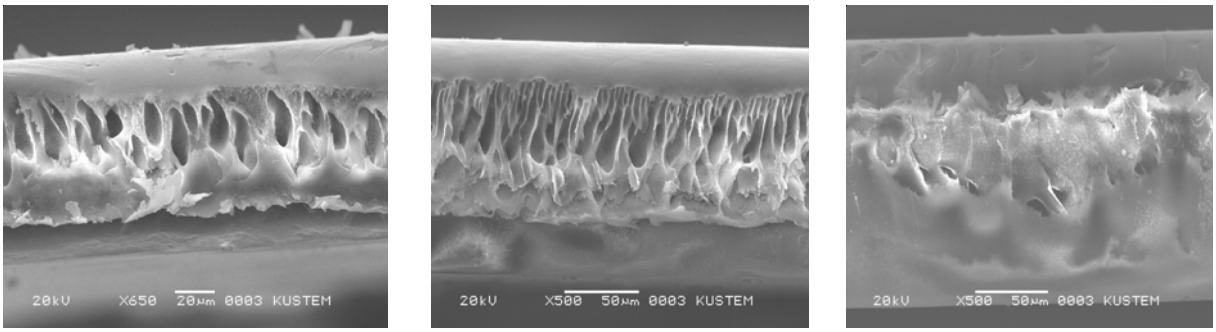

(a) (b) (c)

Fig. 12. Cross-sectional images (a) PSf 18, (b) PSf 20 and (c) PSf 23.

a thin, porous skin layer and comprising regular finger-like voids, penetrated through the whole length of the cross-section. However, PSf 20 membrane shows a finger-like diameter to be narrower and more needle-shaped compared to PSf 18. The formation of the finger-like structure was due to the rapid precipitation of fabricated membranes. This phenomenon was observed when the interfacial nascent membranes were immersed in the first coagulation medium (water bath) which made the membranes having high concentration of H_2SO_4. Then, rapid precipitation occurred in order to leave large voids perpendicular to the film direction.

Membranes produced by casting solution at high level polymer concentrations indicated the increase of the pore size and thicker membranes, including an obvious transition layer supported on a porous substructure. Besides, it would cause changes in the skin thickness, overall membrane porosity and pure water permeability. It was observed clearly that the membrane with the polymer concentration of 23 wt % PSf had changed its pore morphologies from asymmetric, large disruptive macro-voids to symmetric, sponge-like elements. The finger-like pores decreased in size and number due to the increase of polymer concentration. During the phase inversion process, high polymer concentration in casting solution facilitates the formation of a dense surface skin layer supported by a closed-cell substructure. The dense layer was effective in preventing the finger formation and lower diffusion of water into the nascent membrane.

5. Conclusion

The NF membranes with various polymer concentrations were characterized by applying the theoretical approach. Based on the results of the experiment, several conclusions can be drawn as follows:

1) The increase of the polymer concentration tends to exhibit denser membranes.
2) The characterization of the membrane structural details showed great properties in terms of effective pore radius, effective charge density, and ratio of the membrane thickness to the membrane porosity.
3) The electrostatic properties of the membranes were estimated by applying the Teorell–Meyer–Sievers model which is acceptable and withstands in the range of the commercial membranes available in the markets.

Acknowledgement

We greatly acknowledge the financial support from KUSTEM through vote 54160.

Symbols

A_k — Membrane porosity
c — Concentration, mol/m^3
C_i — Concentration in the bulk solution, mol/m^3
c_i — Concentration of component *i,* mol/m^3
$c_{i,p}$ — Concentration of component *I* in the permeate, mol/m^3
C_{total} — Total charge concentration in bulk solution (of –ve or =ve solutes) permeate, mol/m^3
D_i — Diffusivity of ion *i* in free solution, m^2/s
D_s — Solute diffusivity for neutral molecule, or generalized diffusivity for 1–1 type of electrolyte defined as $D_s = 2\,(D_1/D_2)/(D_1+D_2)$, m^2/s
F — Faraday constant, 96487 *C*/mol
H_F,H_D— Steric parameters related to wall correction factors under diffusion and convection conditions, respectively
J_s — Averaged solute flux over membrane surface, mol/m^{3}s
J_v — Averaged solute volume over membrane surface, m/s
k_i — Averaged distribution coefficient of ion *i* by the electrostatic effects
L_p — Pure water permeability, m/s
P — Applied pressure, bar
P_s — Solute permeability, m/s
R — Rejection, %
r — Pore size, m
R_i — Rejection of component *i,* %
r_p — Pore radius, m
r_p — Solute radius, m
S_F, S_D— Distribution coefficient of solute by steric hindrance effect under diffusion and convection condition, respectively
u_x — Velocity in the axial direction to the membrane, m/s
X_d — Effective membrane charge density, mol/m^3
z_i — Valence of ion
Δx — Effective membrane thickness, m

Greek

ε — Membrane porosity (dimensionless
η — Ratio of solute radius to membrane pore radius
σ — Reflection coefficient, %
τ — Tortuosity (dimensioneless
ξ — Ratio of fixed charge density to salt concentration

References

[1] A.F. Ismail and A.R. Hassan, The deduction of fine structural details of asymmetric nanofiltration membranes using theoretical models, J. Membr. Sci., 231 (2004) 25–36.
[2] A.F. Ismail and A.R. Hassan, Formation and characterization of asymmetric nanofiltration membranes: Effects of shear rates and polymer concentration, J. Membr. Sci., 270 (2006) 57–72.
[3] X.L. Wang, T. Tsuru, S.I. Nakao and S. Kimura, Electrolyte transport through nanofiltration membranes by the space–charge model and the comparison with Teorell–Meyer–Sievers model, J. Membr. Sci., 103 (1995) 117–133.
[4] S. Bandini, J. Drei and D. Vezzani, The role of pH and concentration on the ion rejection in polyamide nanofiltration membranes, J. Membr. Sci., 264 (2005) 65–74.
[5] A.E. Yaroshchuk and E. Staude, Charged membranes for low-pressure reverse osmosis properties and applications, Desalination, 86 (1992) 115–134.
[6] M. Mulder, Basic Principles of Membrane Technology. Kluwer Academic, Boston, 1991.
[7] A. Yaroshchuk, Non-steric mechanisms of nanofiltration: Superposition of Donnan and dielectric exclusion, Separ. Purif. Technol., 22–23 (2001) 143–158.
[8] J. Schaep, C. Vandecasteele, A. Mohammad and R. Bowen, Analysis of the salt retention of nanofiltration membranes using Donann steric partitioning pore model, Separ. Sci. Technol., 34 (1999) 309.
[9] X.L. Wang, T. Tsuru., S.I. Nakao and S. Kimura, The electrostatic and steric-hindrance model for the transport of charged solutes through nanofiltration membranes, J. Membr. Sci., 135 (1997) 19–32.
[10] S. Nakao and S. Kimura, Models of membrane transport phenomena and their applications for ultrafil-

tration data, J. Chem. Eng., Japan, 15 (1982) 200.
[11] S. Jain and S.K. Gupta, Analysis of modified suface pore flow model with concentration polarization and comparison with Spiegler–Kedem model in reverse osmosis system, J. Membr. Sci., 232 (2004) 45–61.
[12] M. Perry and C. Linder, Intermediate reverse osmosis ultrafiltration (RO UF) membranes for concentration and desalting of low molecular weight organic solutes, Desalination, 17 (1989) 233–245.
[13] P. Schirg and F. Widmer, Characterisation of nanofiltration membranes for the separation of aqueous dye–salt solutions, Desalination, 89 (1992) 89–107.
[14] A. Chatterjee, A. Ahluwalia, S. Senthilmurugan and S.K. Gupta, Modeling of a radial flow hollow fiber module and estimation of model parameters using numerical techniques, J. Membr. Sci., 236 (2004) 1–16.
[15] S. Wadley, C.J. Brouckaert, L.A.D. Baddock and C.A. Buckley, Modeling of nanofiltration applied to the recovery of salt from waste brine at a sugar decolourisation plant, J. Membr. Sci., 102 (1995) 163–175.
[16] A.L. Ahmad, M.F. Choung and S. Bhatia, Mathematical modeling and simulation of the multiple solutes system for nanofiltration process. J. Membr. Sci., 253 (2005) 103–115.
[17] J. Schaep, B. van der Bruggen, C. Vandecasteele and D. Wilms, Influence of ion size and charge in nanofiltration, Separ. Purif. Technol., 14 (1998) 155–162.
[18] R.W. Bowen, A. Mohammad and N. Hilal, Characterisation of nanofiltration membranes for predictive purpose – Use of salts uncharged solutes and atomic force microscopy, J. Membr. Sci., 126 (1997) 91–105.
[19] R. Gross and J. O'Sterle, Membrane transport characteristics of ultrafine capillaries, J. Chem. Phys., 49(1) (1961) 228.
[20] J.G. Aleman, Modeling of the performance of McMaster pore-filled membranes, PhD dissertation, 2002.
[21] H. Strathmann, K. Kock, P. Amar and R.W. Baker, The formation mechanism of asymmetric membranes, Desalination, 16 (1975) 179–203.
[22] T.H. Young and L.W. Chen, Pore formation mechanism of membranes from phase inversion process, Desalination 103 (1995) 233–237.
[23] O. Kedem and A. Katchalsky, Thermodynamic analysis of the permeability of biological membranes to non-electrolytes, Biochim. Biophys. Acta, 27 (1958) 229.
[24] K.S. Spiegler and O. Kedem, Thermodynamics of hyperfiltration (reverse osmosis): criteria for efficient membranes, Desalination, 1 (1966) 311–326.
[25] E. Gibbin, M. D'Antonio and W.R. Welfoot, Observation on solvent flux and solute rejection acrosssolvent resistant nanofiltration membranes, Desalination, 147 (2002) 307–313.
[26] M. Siddiqiu, G. Amy, J. Ryan and W. Odem, Membrane for the control of natural organic matter from surface waters, Wat. Res., 34 (2000) 3355–3370.
[27] A.F. Ismail and P.Y. Lai, Effects of phase inversion factors on formation of defect-free and ultrathin-skinned asymmetric polysulfone membranes for gas separation. Separ. Purif. Technol., 33 (2003) 127–143.